Open Access

OBM Genetics

LIDSEN Publishing Inc.

Research Article

Arginine and Histidine-modified Layered Double Hydroxides Facilitate Transgene Expression in Cancer Cells in Vitro

Nirasha Nundkumar [1, †], Sooboo Singh [2, †], Moganavelli Singh [1, †, *]

1. Nano-Gene and Drug Delivery Group, Discipline of Biochemistry, University of KwaZulu-Natal, Private Bag X54001, Durban, South Africa; E-Mails: Nundkumar@ukzn.ac.za; singhm1@ukzn.ac.za
2. School of Chemistry and Physics, University of KwaZulu-Natal, Private Bag X54001, Durban, South Africa; E-Mail: singhso@ukzn.ac.za

† These authors contributed equally to this work.

* **Correspondence:** Moganavelli Singh; E-Mail: singhm1@ukzn.ac.za

Academic Editor: Ying S. Zou

Special Issue: Gene Therapy on Cancer

OBM Genetics
2023, volume 7, issue 3
doi:10.21926/obm.genet.2303193

Received: June 14, 2023
Accepted: September 18, 2023
Published: September 21, 2023

Abstract

Layered double hydroxides (LDHs) have interesting properties and structures that enable them to carry nucleic acids, such as deoxyribonucleic acid (DNA). This study synthesized LDHs using the co-precipitation method and functionalized with the amino acids arginine (Arg) and histidine (His) to promote proton-sponge activity for enhanced transgene expression. The LDHs were characterized using X-ray diffraction (XRD), transmission electron microscopy (TEM), and nanoparticle tracking analysis (NTA). The interaction of the LDHs with the reporter gene plasmid DNA (*pCMV-Luc DNA*) was determined using agarose gel electrophoresis. Cytotoxicity and transgene expression was assessed using the 3-(4, 5-dimethylthiazol-2-yl)-2.5-diphenyltetrazolium bromide (MTT) and luciferase reporter gene assay in the human embryonic kidney (HEK293), colorectal carcinoma (Caco-2) and hepatocellular carcinoma (HepG2) cells. The DNA: LDH complexes were relatively non-cytotoxic to all cells, and the

highest transgene expression was achieved in the HEK293 cells exhibiting the most significant degree of transfection, followed by the Caco-2 cells. The His-LDH complexes displayed more than a two-fold increase in transfection than the Arg-LDHs, especially in the HEK293 cells at the optimal binding ratio. The non-functionalized LDHs demonstrated high transfection, which exceeded that of the His-LDH and Arg-LDH by 20% and 30%, respectively, in the Caco-2 cells. Little difference was noted in the HepG2 cells, which presented with the lowest transfection. These LDHs have demonstrated the potential to bind, protect, and efficiently deliver pDNA *in vitro*.

Keywords
Layered double hydroxide; histidine; arginine; cytotoxicity; transgene expression; DNA

1. Introduction

Gene therapy is continually evolving, with gene delivery remaining the most significant challenge. Naked nucleic acids cannot easily traverse the cell membrane, partly due to their negative charge, and even when they do enter the cell, they are prone to degradation by nucleases in the body. Hence, the challenge lies in safely delivering the therapeutic nucleic acid into the cell for gene therapy. A suitable carrier is required to protect and transport the nucleic acid into the cell efficiently. The popular vehicle used to date has been of viral origin. These viral vehicles have several drawbacks, including immunogenic responses, low DNA loading, insertional mutagenesis, lack of specific cell targeting, and high cost [1]. Hence the shift to non-viral vehicles was expected, with carriers such as liposomes [2-6], gold nanoparticles [7, 8], dendrimers [9, 10], quantum dots [11], carbon nanotubes [12-14], magnetic nanoparticles [15] and functionalized polymers [10, 16, 17], being explored in gene therapy. However, these carriers produce lower transfection efficiencies than their viral counterparts. Thus, further optimization of these carriers is required.

An ideal gene delivery vehicle must bind and adequately protect the therapeutic cargo, traverse the cell membrane, have site-specific delivery, and produce suitable transfection without adverse effects on the cell [18, 19]. Layered double hydroxides (LDH), known as hydrotalcite or hydrotalcite-like materials, have been explored as gene delivery vehicles [20, 21] due to their unique and highly tunable properties. Nucleic acids can be easily incorporated into LDHs by ion exchange, intercalation, or adsorption [22]. The nano complex formed gains extra stabilization energy due to the electrostatic interaction between the cationic brucite layers and the nucleic acid [23]. The positively charged atoms on the LDH surface interact with the negatively charged cell membrane, leading to the internalization of the nanocomplex.

Early endosomal escape is a limiting step in gene therapy. Better transfection may be achieved by manipulating or functionalizing the carrier to facilitate endosomal escape. Xu and coworkers have used the addition of amino groups for better interaction with the DNA chains [24] due to the presence of terminal amino groups that would react favorably with the DNA. Arginine (Arg) and histidine (His) are amino acids that are positively charged at physiological pH. Functionalization with arginine or histidine could improve the LDH interaction with the DNA and the cell membrane and facilitate endosomal escape due to the enhancement of the 'proton sponge' effect. Guanidinium-

containing amino acids, such as Arg, have been incorporated into cell-penetrating peptides, as they are known to quickly traverse the cell membranes, leading to the efficient delivery of their cargo into the cell cytoplasm [25]. The essential amino acid, His that possess an imidazole group has favorable properties that include proton buffering, metal ion chelation, and antioxidant activity [26]. Amino acid functionalized hydrotalcite [27] have been reported to induce gene silencing in vitro successfully. In the current study, we compare the transfection efficiency of unfunctionalized and arginine and histidine-functionalized LDHs to deliver pCMV-Luc DNA (pDNA). The use of amino acid-functionalized LDHs has not yet been fully exploited in gene therapy. This proof of concept study lays the basis for using these functionalized LDHs in therapeutic gene delivery.

2. Materials and Methods

2.1 Materials

Ethidium bromide, phosphate-buffered saline (PBS) tablets, MTT salt (3- (4, 5-dimethylthiazol-2-yl)- 2, 5-diphenyltetrazolium bromide) and ethylenediaminetetraacetic acid (EDTA) (disodium salt, dihydrate), $Mg(NO_3)_2{\cdot}6H_2O$, $Al(NO_3)_3{\cdot}9H_2O$, NaOH and Na_2CO_3 were acquired from Merck, Darmstadt, Germany. DNA grade agarose was obtained from Bio-Rad Laboratories, Richmond, USA. L-arginine, L-histidine, and bicinchoninic acid (BCA) assay reagents were obtained from Sigma-Aldrich, St Louis, MO, USA. The Luciferase assay kit was purchased from the Promega Corporation, Madison, USA. Eagle's Minimum Essential Medium (EMEM), trypsin-versene, and penicillin-streptomycin were purchased from Lonza BioWhittaker (Walkersville, USA). Fetal bovine serum (FBS) was supplied by Hyclone GE Healthcare (Utah, USA). Corning Inc. (NY, USA) provided all the sterile tissue culture plasticware. The human embryonic kidney (HEK293), colon adenocarcinoma (Caco-2), and hepatocellular carcinoma (HepG2) cells were procured directly from the American Type Culture Collection, Manassas, VA, USA, and used after their second passage.

2.2 Synthesis of LDHs

The LDHs and amino acid functionalized LDHs (aa-LDHs) were prepared using the co-precipitation technique at low supersaturation, using MII:MIII ratios of 2:1 and 3:1 and M^{II}:M^{III}: aa ratios of 2:1:1 and 3:1:1. For Mg-Al with MII:MIII ratio of 2:1 (MgAl 0.33), 0.1 mol $Mg(NO_3)_2{\cdot}6H_2O$ and 0.05 mol $Al(NO_3)_3{\cdot}9H_2O$ were dissolved in 200 mL deionized water. This was added dropwise to Na_2CO_3 (0.5 M), with vigorous stirring, maintaining a pH of 11. The final suspension was heated to 80°C under reflux for 18-20 h. The precipitate was filtered, washed until the filtrate had a pH of 7, and dried in a 110°C oven overnight. The resulting residue was ground to a fine powder (talc-like consistency). Mg-Al LDH with M^{II}:M^{III} (3:1; MgAl 0.25) and the aa-LDHs were prepared as above. The aa-LDHs were prepared in the molar ratios Mg:Al:aa of 2:1:1 (denoted MgAlArg 0.33 and MgAlHist 0.33) and Mg:Al:aa of 3:1:1 (denoted MgAlArg 0.25 and MgAlHist 0.25).

2.3 Characterization of LDHs

The LDHs and aa-LDHs were characterized using powder X-ray diffraction (XRD), inductively coupled plasma-optical emission spectroscopy (ICP-OES), Fourier transform infrared spectroscopy (FTIR), transmission electron microscopy (TEM), scanning electron microscopy (SEM) and Nanoparticle Tracking Analysis (NTA).

XRD was obtained using a Bruker D8 Advance diffractometer with a graphite monochromator operating at 40 kV and 40 mA. ICP was conducted on a Perkin Elmer Optical Emission Spectrometer Optima 5300 DV and FTIR using a Perkin Elmer Spectrum Universal ATR 100 FT-IR Spectrometer. TEM and SEM were performed using a JEOL 1010 Megaview 3 Soft Imaging system and a LEO 1450 SEM instrument. NTA provided the particle size and zeta (ζ)-potential (NanoSight NS500; Malvern Instruments Ltd., Worcestershire, UK). The ultrastructural morphology, size, and ζ-potential of the pDNA: LDH complexes were also determined using TEM, XRD, and NTA, respectively. The qualitative ninhydrin test was used to confirm the presence of amino acids in the aa-LDHs. The amount of Arg in the MgAlArg 0.25 and MgAlArg 0.33 was determined using a spectrophotometric method by Wang and coworkers [28]. Histidine quantification in MgAlHist 0.25 and MgAlHist 0.33 was achieved using the technique described by Patel and coworkers [29].

2.4 pDNA Binding Studies

This assay was based on the electrophoretic mobility shift assay described in the literature [30]. To confirm the optimal binding of the pDNA to the LDH, 0.5 µg of pCMV-*Luc* DNA was added to varying amounts of the respective LDH, mixed, and kept at room temperature for 10 min. After that, 2 µl of gel loading buffer was added to each sample, followed by a 1% agarose gel electrophoresis at 50 V for 90 minutes. Gels were viewed, and images were captured using a Syngene G-Box imaging system (Syngene, Cambridge, UK). The ratio below the optimal pDNA: LDH ratio will be referred to as the sub-optimal ratio, and the ratio above the optimal will be referred to as the supra-optimal ratio.

2.5 Nuclease Protection Assay

This assay was conducted as described previously [30]. The pDNA: LDH (10 µl) complex was prepared at the optimal binding ratio determined in the binding studies (section 2.4). Two control samples were also prepared: a positive control containing only pDNA and a negative control containing pDNA and 10% (v/v) FBS. The FBS was also added to the nanocomplex, and all samples were incubated at 37°C for four h. The enzyme reaction was stopped by adding ethylenediamine tetra-acetic acid to a final concentration of 1 mM. The sample was then centrifuged, and 0.1 M HCl (1 µl) was added to the pellet, which was incubated at 37°C for one h, followed by electrophoresis as in section 2.4.

2.6 Cytotoxicity

Cells (Caco-2, HEK293, and HepG2) were maintained in EMEM supplemented with 10% (v/v) FBS and 1% antibiotics (100 U/ml penicillin, 100 µg/ml streptomycin) at 37°C and 5% CO_2, in a HEPA Class 100 Steri-Cult CO_2 incubator (Thermo-Electron Corporation, Waltham, Massachusetts, USA). Cells were seeded into 48-well plates at 3×10^4 cells/well density and incubated at 37°C for 24 hours. The medium was then replenished, and the pDNA:LDH complexes (at sub-optimal, optimal, and supra-optimal binding ratios) were added, and cells were incubated for 48 hours at 37°C. A positive control containing only cells was set as 100% cell viability. All assays were performed in triplicate. After the 48-hour incubation period, the medium was removed, and 200 µl medium and 20 µl MTT reagent (5 mg/ml in PBS) were added to each well. The cells were incubated at 37°C for 4 hours,

after which the MTT-medium solution was removed, and 200 µL DMSO was added to solubilize the formazan crystals. Absorbance was read at 540 nm using a Mindray MR-96A microplate reader (Vacutec, Hamburg, Germany).

2.7 Transfection Studies

Transfection studies were carried out *in vitro*, using the reporter plasmid, pCMV-*Luc* DNA. The cells (HEK293, HepG2, and Caco-2) were seeded and treated with the pDNA:LDH complexes as for the cytotoxicity study and incubated for 48 h at 37°C. Assays were done in triplicate. Two controls were used, cells only and cells treated with naked pCMV-*Luc* DNA. Following incubation, the luciferase activity of the cells was determined using the Promega luciferase assay system. The medium was removed, and cells were washed twice with PBS. Thereafter, 80 µl of 1× cell lysis reagent (25 mM Tris-phosphate, pH 7.8; 2 mM dithiothreitol, 2 mM 1,2- diaminocyclohexane - N, N, N'N'- tetra-acetic acid, 10% (v/v) glycerol, 1% (v/v) triton X-100) was added to the cells, which were gently shaken for 15 minutes. The lysed cells were pelleted at 12000 xg for 5 seconds. The supernatant (20 µl) was added to 100 µl luciferase assay reagent (20 mM Tricine, 1.1 mM magnesium carbonate hydroxide pentahydrate, 2.7 mM magnesium sulfate, 0.1 mM EDTA, 33.3 mM dithiothreitol, 270 µM coenzyme A, 470 µM luciferin, 530 µM ATP) and measured for luminescence in a GloMax® multi detection system (Promega BioSystems, Sunnyvale, USA). The BCA assay determined the protein content, and luminescence readings were normalized against the protein content and expressed as relative light units per milligram protein (RLU/mg protein).

3. Results

3.1 Synthesis and Characterization

The LDHs and aa-LDHs were successfully synthesized using the co-precipitation method. LDHs denoted with "0.25" indicate a mole ratio of 3:1 (M^{2+}:M^{3+}), and those with "0.33" indicate a mole ratio of 2:1 (M^{2+}:M^{3+}). The MgAl 0.25, MgAl 0.33, MgAlArg 0.25, MgAlArg 0.33, MgAlHist 0.25, and MgAlHist 0.33 samples were all pristine white, talc-like powders, insoluble in water, forming suspensions. The ninhydrin test confirmed the presence of Arg and His, and the percentage incorporation of amino acid was calculated to be 0.90% in MgAlHist 0.25, 1.89% in MgAlHist 0.33, 1.27 % in MgAlArg 0.25 and 2.62 % in MgAlArg 0.33.

The XRD diffractograms for the LDHs and aa-LDHs corresponded to those of LDHs (ICDD 01-089-5434) (Supplementary Figure S1). The values for the “a”, “d” and “c” lattice parameters are indicated in Table 1. MgAl (0.25) and MgAl (0.33) differ from each other due to the content of the M(II) and M(III) metal ions. However, this does not impact the geometry of the material, clearly indicated by its lattice parameters. Adding the amino acids into the layered double hydroxides causes a slight increase in the lattice parameters, which also does not alter the geometry of the materials. The LDHs display more substantial peaks at (003) and (006), with lesser peaks at (012), (015), (018), (100), and (113), similar to that reported in the literature [27, 31, 32]. A shift in the peaks due to the presence of histidine and arginine was noted.

Table 1 The lattice parameters of all the materials generated from XRD analysis.

Sample	Lattice parameters		
	a(Å)	c(Å)	d_{003}(Å)
MgAl (0.25)	3.11	23.15	7.56
MgAl (0.33)	3.11	23.15	7.56
MgAlArg (0.25)	3.11	23.18	7.63
MgAlArg (0.33)	3.11	23.17	7.62
MgAlHis (0.25)	3.11	23.17	7.59
MgAlHis (0.33)	3.11	23.20	7.66

FTIR Supplementary Figure S2 confirmed the presence of specific functional groups present in the LDHs. The OH-stretching is evident at 3440 cm^{-1}. The band for the interlayer water bending is around 1650 cm^{-1}, indicating water's role in the LDH structure. Intercalated anions produced bands between 1800-1000 cm^{-1}. Stretching of the interlayer carbonate ions is evident between 1300 and 1400 cm^{-1}. The OH groups joined to the carbonate ions are stretching around 3100 cm^{-1}. Lesser CO_3^{2-} vibrations are observed around 730 cm^{-1}, 850 cm^{-1}, and 1000 cm^{-1}. All assignments were done according to that reported in the literature [27, 33-36]. For the aa-LDHs, O-H stretching was seen from around 3400 cm^{-1}, carbonate ion stretching from 1300 cm^{-1} onwards, with low-frequency M-O (metal-oxygen) and M-O-M vibrations from 400 cm^{-1} to 800 cm^{-1} [33, 37, 38], similar to unmodified LDHs. The bands at 2943 cm^{-1} and 2933 cm^{-1} for the arginine-LDHs correspond to the asymmetric stretching of the methyl groups of arginine [39].

TEM revealed typical LDH morphologies (Figure 1). TEM analysis of the pDNA:LDH complexes (Figure 2) revealed compact complexes with diameters ranging from 10-250 nm. Some complexes displayed an almost 'square' or "cube" shaped morphology, while others appeared hexagonal.

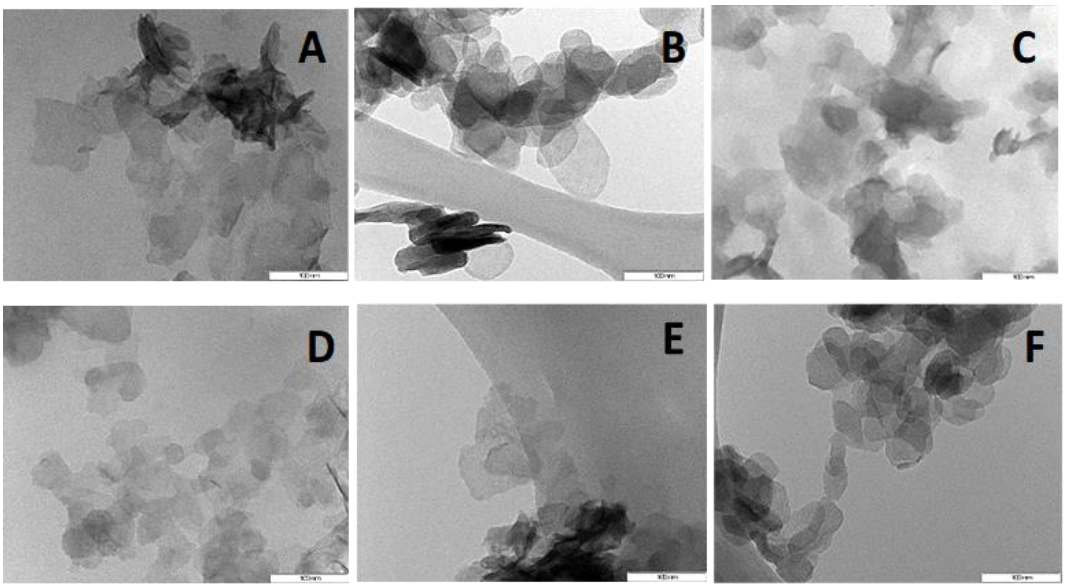

Figure 1 TEM images: (A) MgAl 0.25; (B) MgAl 0.33; (C) MgAlArg 0.25; (D) MgAlArg 0.33, (E) MgAlHist 0.25 and (F) MgALHist 0.33 at 300 K magnification. Bar = 100 nm.

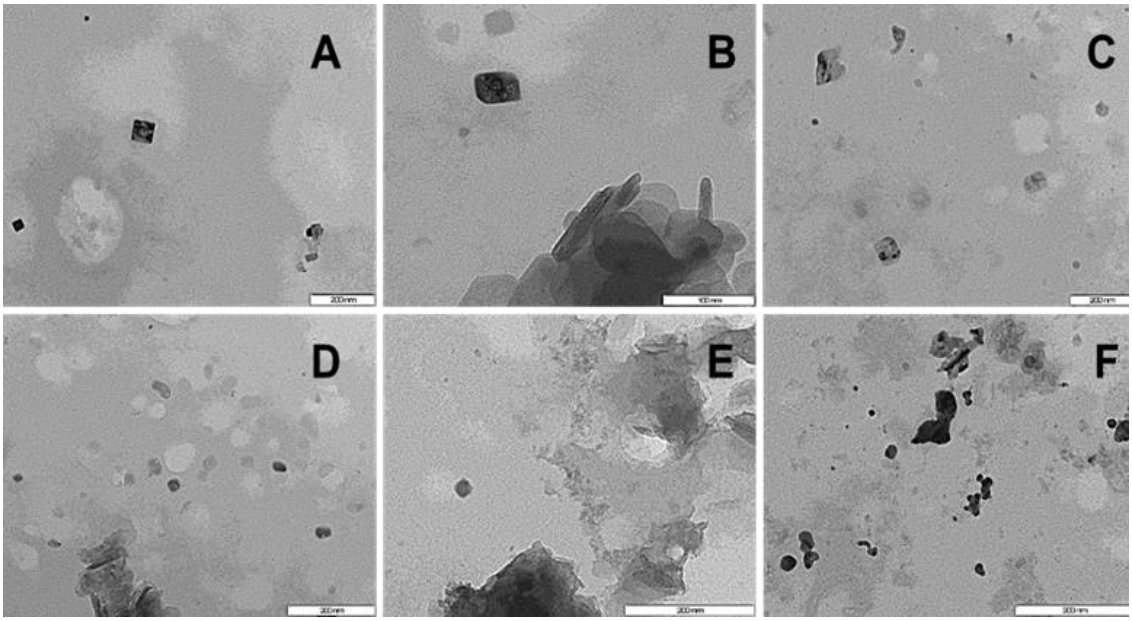

Figure 2 TEM images of pDNA:LDH complexes with (A) MgAl 0.25 at 60K magnification, (B) MgAl 0.33 at 200K magnification, (C) MgAlArg 0.25 at 100K magnification, (D) MgAlArg 0.33 at 150K magnification, (E) MgAlHist 0.25 at 200K magnification and (F) MgAlHist 0.33 at 200K magnification. Bar = 200 nm.

From NTA, the sizes of the LDHs ranged from 44.5-141 nm and the zeta potentials from 6.7 to 22.7 mV, while complexes ranged from 25.1 to 80.1 nm in length, with zeta potentials from -19.8 to -28 mV (Table 2).

Table 2 Size and zeta potential of the LDHs and pDNA:LDH complexes obtained from NTA.

LDH	PARENT LDH		pDNA: LDH COMPLEXES	
	SIZE (nm)	ZETA POTENTIAL (mV)	SIZE (nm)	ZETA POTENTIAL (mV)
MgAl 0.25	141	17.1	80.1	-19.8
MgAl 0.33	72.4	15.0	25.1	-21.3
MgAlArg 0.25	125.1	21.9	26.9	-11.8
MgAlArg 0.33	123.7	6.7	30.8	-27.3
MgAlHist 0.25	75.2	21.2	34.6	-28.0
MgAlHist 0.33	44.5	22.7	53.9	-23.5

3.2 DNA Binding

All LDHs displayed complete binding with pDNA at a ratio of pDNA:LDH of 1:30 (Figure 3).

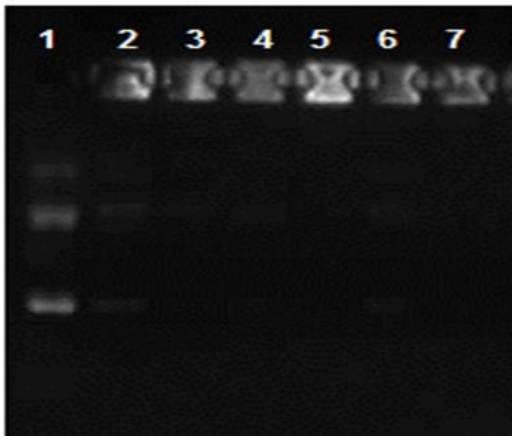

Figure 3 Gel retardation studies: pDNA only (lane 1), pDNA:MgAl 0.25 (lane 2), pDNA:MgAlArg 0.25 (lane 3), pDNA:MgAlHist 0.25 (lane 4), pDNA:MgAl 0.33 (lane 5), pDNA:MgAlArg 0.33 (lane 6), pDNA:MgAlHist 0.33 (lane 7). All complexes were prepared in a ratio of pDNA:LDH of 1:30 (w/w) and formed electroneutral complexes that were retained in the wells.

From Figure 3, the unbound pDNA in lane 1 (control) migrated freely into the gel, and the bands showing the linear, supercoiled, and circular DNA forms are visible. Upon binding of the pDNA to the LDHs, electroneutral complexes are formed, and the DNA's movement into the gel is retarded [30]. The LDH:pDNA complexes remain in the wells, as evidenced by the fluorescence in lanes 2 to7. These are the optimal binding ratios.

The actual mode of binding in this study was investigated further using XRD (Figure 4). There was a slight shift in the 2θ values of the (003) and (006) planes of the LDH in the XRD diffractogram of the pDNA:MgAl 0.33 complex, indicating probable intercalation of the amino acid has occurred.

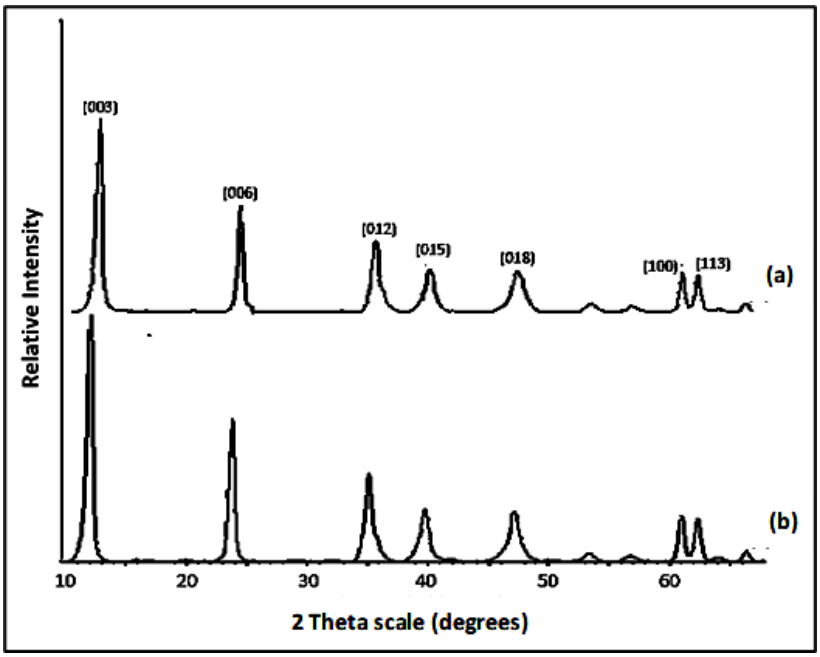

Figure 4 XRD pattern of (a) MgAl 0.33 (b) pDNA:MgAl 0.33 complex.

3.3 Nuclease Digestion

This assay was performed using only the pDNA:MgAl 0.33 complex, as all the nucleic acid:LDH complexes would be expected to react similarly when exposed to serum nucleases. From the results obtained (Figure 5), it can be seen that the pDNA:LDH complex does offer some degree of protection to the pDNA from serum nucleases.

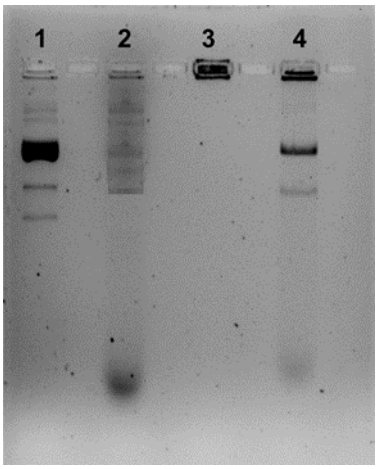

Figure 5 Nuclease digestion assay of pDNA:MgAl 0.33. Lane 1: naked pDNA, Lane 2: pDNA exposed to nuclease digestion, Lane 3: MgAl 0.25: pDNA complex, and Lane 4: MgAl 0.25: pDNA complex exposed to nuclease digestion.

The naked, unprotected pDNA (lane 2) was degraded upon exposure to serum nucleases. For the pDNA:LDH complexes, the pDNA retained its integrity, with the bands of the linear, circular, and supercoiled forms of the pDNA still being quite clearly visible (lane 4). Some of the pDNA:LDH complex remained in the well, as was also reported by Kriven and coworkers [40], who suggested that pDNA can only be wholly released from the complex at a pH of 2 or less.

3.4 Cytotoxicity

All cell lines tolerated the Mg-Al based pDNA:LDH complexes very well at the ratios and conditions tested (Figure 6). The cell viabilities, after a 48 hour incubation period with complexes prepared at optimal ratio were, for Caco-2 cells -MgAl 0.25 (83.50%), MgAl 0.33 (91.16%), MgAlArg 0.25 (105.2%), MgAl Arg 0.33 (102.9%), MgAlHist 0.25 (103.3%) and MgAlHist 0.33 (102.8%); for the HEK293 cells -MgAl 0.25 (103.7%), MgAl 0.33 (99.69%), MgAlArg 0.25 (98.58%), MgAl Arg 0.33 (102.1%), MgAlHist 0.25 (105.3%) and MgAlHist 0.33 (109.8%); and for the HepG2 cells - MgAl 0.25 (97.57%), MgAl 0.33 (101.5%), MgAlArg 0.25 (108.3%), MgAl Arg 0.33 (103.5%), MgAlHist 0.25 (109.1%) and MgAlHist 0.33 (106.3%) respectively.

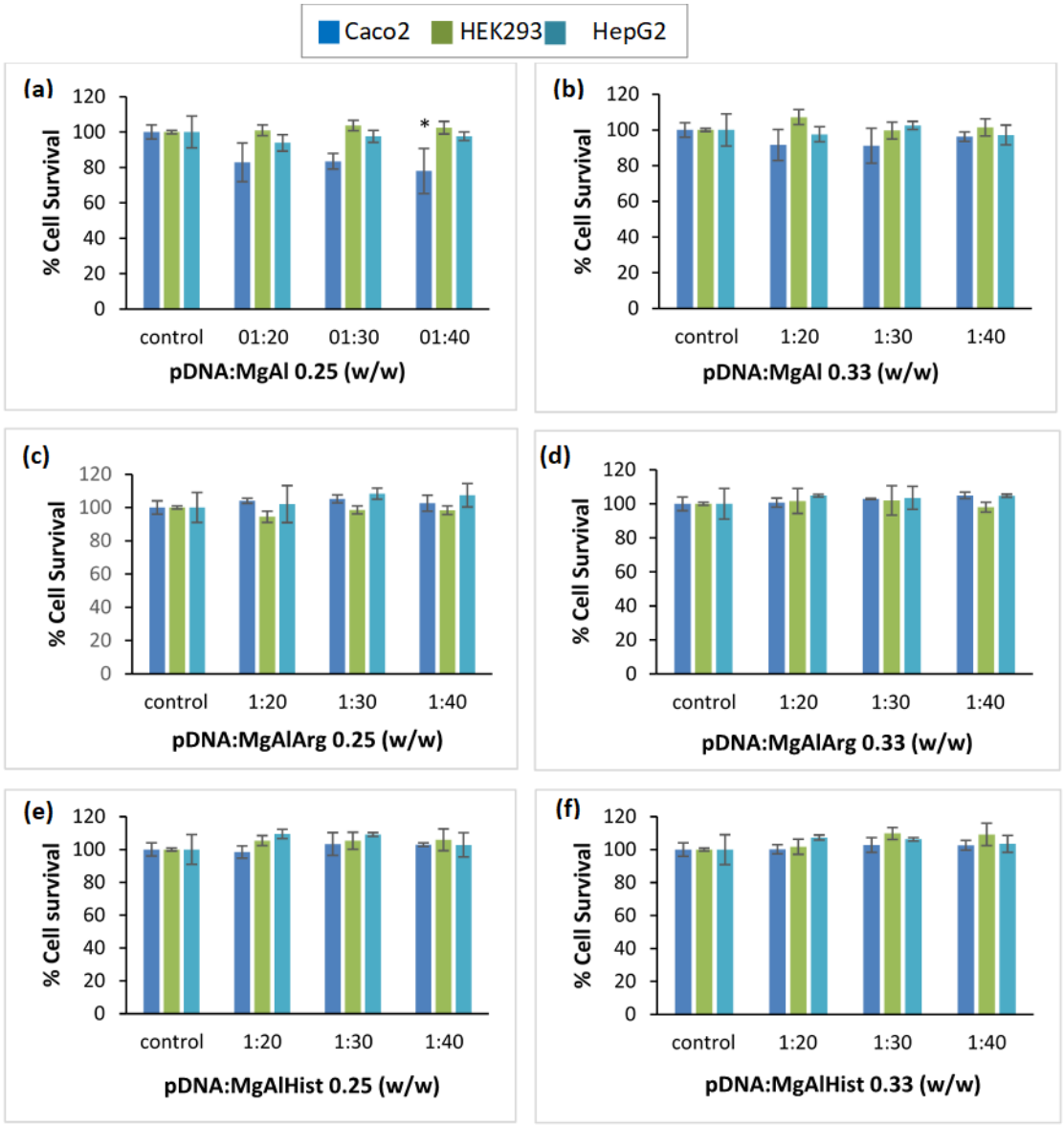

Figure 6 MTT assay of Caco-2, HEK293 and HepG2 cells exposed to (a) pDNA:MgAl 0.25 complexes, (b) pDNA:MgAl 0.33 complexes, (c) pDNA:MgAlArg 0.25 complexes, (d) pDNA:MgAlArg 0.33 complexes, (e) pDNA:MgAlHist 0.25 complexes and (f) pDNA:MgAlHist 0.33 complexes. Data are represented as means ±SD (n = 3). *$p < 0.05$ was considered statistically significant.

The Tukeys comparison test revealed no statistical significance, except in the case of MgAl 0.25 at the supra-optimal binding ratios. Minimal cell death was observed with the Caco-2 cell line after treatment with all the complexes, but the presence of the complexes appeared to be growth-promoting in the HEK293 and the HepG2 cell lines. The complexes appeared to 'shroud' the cells, protecting them and promoting cell growth.

3.5 Transfection Studies

The level of luciferase gene expression in all cell lines tested indicated successful transfection, with the degree of transfection being cell type dependent (Figures 7-9). The Caco-2 cells (Figure 7)

showed low but promising gene expression, while the HEK293 cells (Figure 8) displayed the highest luciferase gene expression. The HepG2 cells (Figure 9) showed minimal gene expression, approximately 800-fold less than that indicated by the HEK293 and Caco-2 cells. In the Caco-2 cell line, the luciferase activity was as follows: MgAlArg 0.25 < MgAlHist 0.25 < MgAlArg 0.33 < MgAl 0.25 < MgAlHist 0.33 < MgAl 0.33. In the HEK293 cell line, the luciferase activity was as follows: MgAlArg 0.25 < MgAl 0.25 < MgAlArg 0.33 < MgAlHist 0.25 < MgAlHist 0.33 < MgAl 0.33.

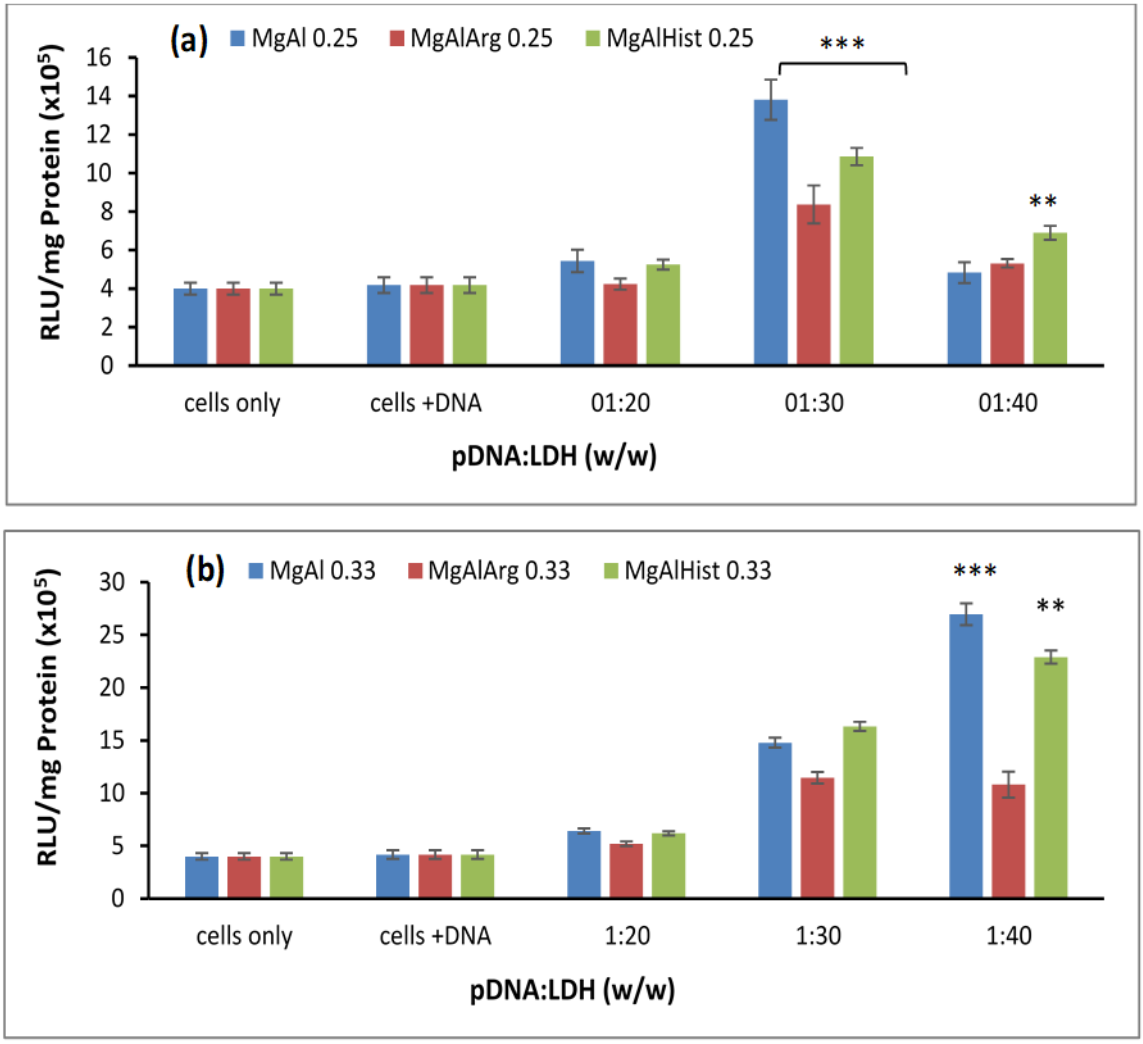

Figure 7 Luciferase gene expression in Caco-2 cells using (a) MgAl 0.25, MgAlArg 0.25 and MgAlHist 0.25 and (b) MgAl 0.33, MgAlArg 0.33 and MgAlHist 0.33. Two sets of controls were used; one containing only Caco2 cells and the second control containing cells treated with pCMV-*Luc* DNA. The data are represented as means ±SD (n = 3). **p < 0.005, ***p < 0.0005 was considered statistically significant.

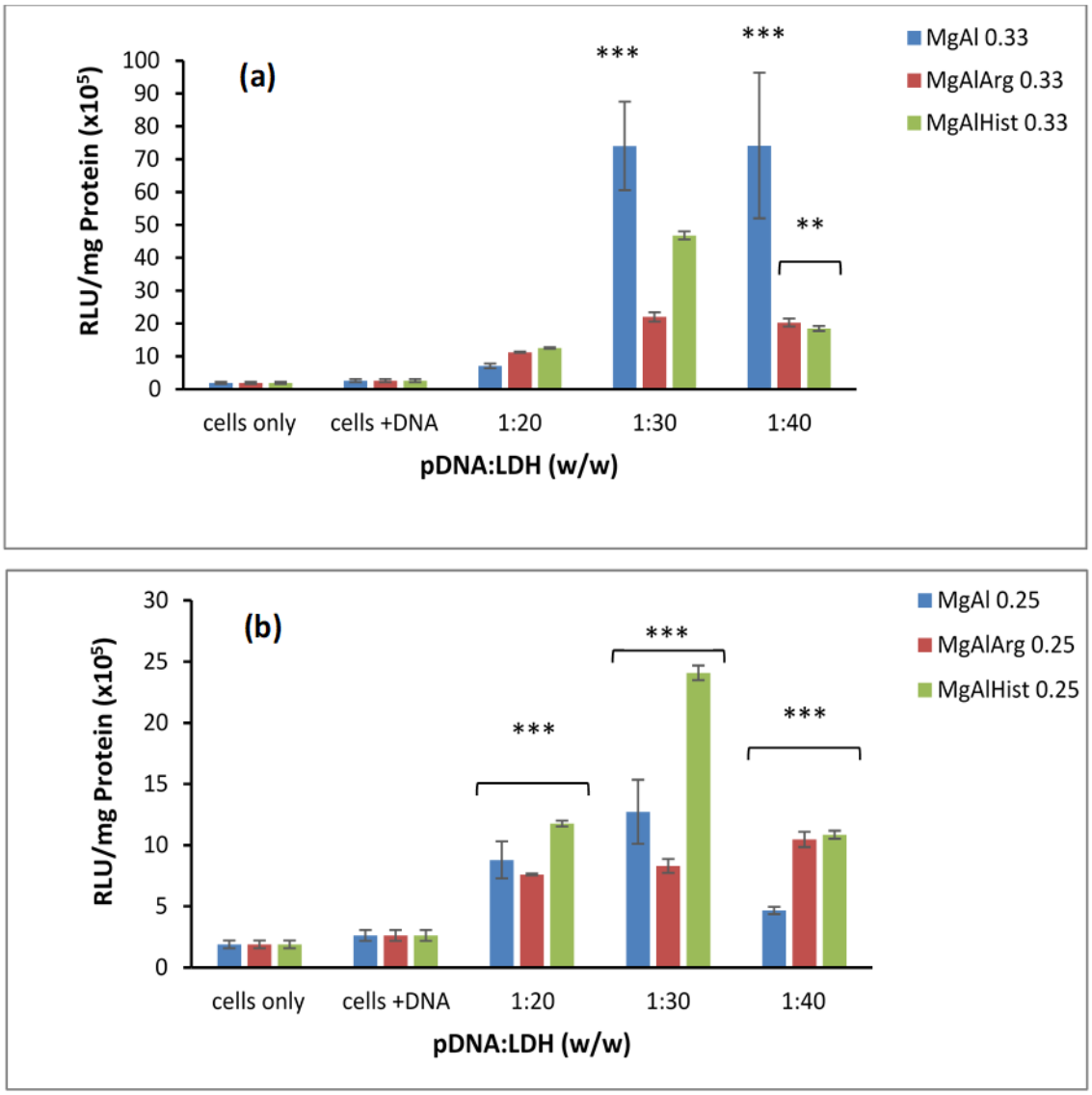

Figure 8 Luciferae gene expression in HEK293 cells using (a) MgAl 0.25, MgAlArg 0.25 and MgAlHist 0.25 and (b) MgAl 0.33, MgAlArg 0.33 and MgAlHist 0.33. Two sets of controls were used; one containing only HEK293 cells and the second control containing cells treated with pCMV-*Luc* DNA. Data are represented as means ±SD (n = 3). **p < 0.005, ***p < 0.0005 was considered statistically significant.

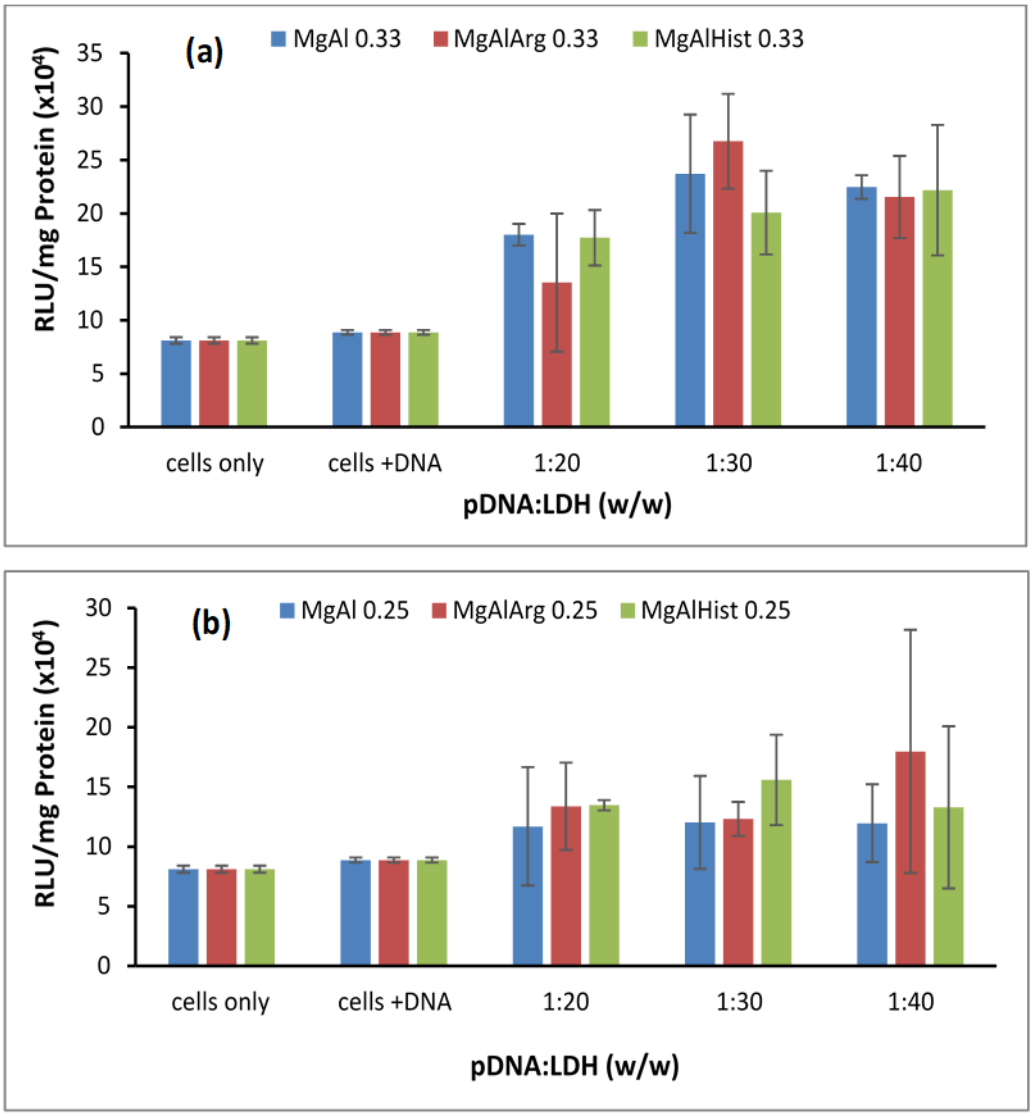

Figure 9 Luciferase gene expression in the HepG2 cells using (a) MgAl 0.25, MgAlArg 0.25 and MgAlHist 0.25 and (b) MgAl 0.33, MgAlArg 0.33 and MgAlHist 0.33. Two sets of controlswere used; one containing only HepG2 cells and the second control containing cells treated with pCMV-*Luc* DNA. Data are represented as means ±SD (n = 3). No significant transfection was observed.

The non-functionalized MgAl 0.25 generally exhibited low luciferase expression in all cells. The non-functionalized LDHs and the aa-LDHs in ratios of 2:1 displayed significantly higher transfection activity than those in the 3:1 ratio. The use of the MgAl 0.33 LDH resulted in the highest level of transfection in all cells. Histidine-functionalized LDHs displayed better transfection efficiency than arginine-functionalized LDHs in the Caco-2 and HepG2 cells.

4. Discussion

XRD confirmed the crystalline nature of the LDHs, while FTIR indicated the presence of the important functional groups in the LDHs and the interlayer anions. However, some of the bands that may be commonly observed for the amino acids histidine and arginine were not very visible due to

possible masking by the water present within the layers [19, 41] or due to the small amount of each amino acid that was incorporated into the LDHs. TEM further showed LDHs of different shapes but sizes smaller than those obtained by NTA. This could be attributed to the various preparation processes used, with TEM measuring the LDHs in their dry state while NTA examined them in an aqueous solution [42], similar to what one would encounter in an *in vivo* environment.

The size of a nanoparticle plays a vital role in the cellular uptake of the particles [43, 44]. It was reported that for maximum cellular uptake with minimal toxicity, LDH sizes should be between 50 and 100 nm [45]. In some cases, the pDNA:LDH complexes in this study were smaller than that of the parent LDHs, with the complexes all below 100 nm except for the pDNA:MgAl 0.25 which was above 150 nm. Hence, the sizes of these pDNA:LDH complexes are suitable for cellular uptake. The zeta potential provides a good indication of the colloidal stability of the nanoparticles for in vivo application. Although these nanocomplexes displayed a negative zeta potential at pH 7, the zeta potential may be altered at physiological pH, resulting in reduced effects on the transfection efficacy. Negative zeta potentials are expected to lead to poor cellular uptake and transfection. Zeta potential is not necessarily an indication of the actual surface charge of the nanoparticle. It measures the potential difference between the particle surface and the solvent and is dependent on other factors, such as the pH of the solvent [46]. Desigaux and coworkers have previously hypothesized that a negative zeta potential would not impede cellular internalization [47], although a positive zeta potential would favor cellular uptake.

Overall, there was efficient binding of the pDNA to the LDHs. It has been suggested that the high energy transmitted during vortexing harmonizes the interaction between the nucleic acid and the carrier vector [48], favoring the complete binding of the DNA. It is possible that during complex formation between the pDNA and LDHs, a loss of water molecules from the interlayer could lead to a decrease in interlayer spacing, partially or fully "trapping" the pDNA and enhancing complex formation [49]. Another possible mechanism is that electrostatic forces bind the LDH surfaces to the phosphate backbone of the DNA [43]. The phosphate oxygen forms co-ordination metal-oxygen-phosphate bonds, resulting in the adsorption of DNA onto the outer surface of the LDH. The binding of the pDNA to the external surface of the LDH was previously observed [43, 50]. It has been reported that nucleic acid binding can occur due to ion exchange with interlayer anions [24]. The negative zeta potentials of most of the pDNA:LDH complexes suggest that the pDNA was adsorbed onto the surfaces of the LDH rather than intercalated within the layers.

Most compaction occurs during complex formation, which is evident when looking at the sizes of the naked pDNA and LDH to the pDNA:LDH complexes. This compaction occurs due to the electrostatic interaction between the cations on the LDH surface and the anionic phosphate backbone of the pDNA [51]. The phosphate groups of the pDNA are electrostatically neutralized by associating with the cations on the LDH molecules, leading to a condensed, more stable complex structure, the shape of which depends on the extent of condensation. The pDNA intercalation within the interlayer would have resulted in an increase in d003 to 23.7 Å, which is the diameter of the pDNA [52]. The unchanged d003 value in the pDNA:MgAl 0.33 complex confirmed that the pDNA binds to the outer surfaces of the LDH. The slight shift to the right of the diffraction peaks of the MgAl 0.33:pDNA complex most probably occurs due to the pDNA binding to the outer surface of the LDH.

The mechanism of release of the pDNA from the pDNA:LDH complex has been proposed to occur via dissolution in the endosome due to low pH [23, 52]. LDHs begin to dissolve in a pH range of 4-5,

releasing their cargo in a pH-dependent manner [53]. The buffering capacity of LDHs has been well documented. This property has been exploited in producing antacids from LDHs for years [54]. It has also been reported that hydrotalcite can buffer the stomach's contents at pH 4 for extended periods [55]. This property has also made LDHs increasingly attractive for medical applications, where they can be used for the controlled release of medicines. Thus, the incomplete release of the pDNA from the complex in the nuclease digestion assay can be expected after an overnight incubation period. The slow dissolution process of the pDNA:LDH complex alludes to the transfection rate of the LDH complexes being slow**.**

Cytotoxicity of nanoparticles is influenced by several factors, such as the cell line used, cell culture conditions, type of assay used, nanoparticle size, nanoparticle concentration, and duration of exposure [56]. Balcomb and coworkers reported similar results and suggested that the increased cell viabilities, especially with iron-containing LDHs, were possibly due to the increased redox potential and cell oxidative processes within the cell due to increased intracellular iron [21]. The overall good cell viability bodes well for using these LDHs in gene delivery, as they will ensure the safe delivery of the gene with little or no side effects.

The different cell lines used in this study showed varied luciferase expression levels. This variation could be due to the different cell types' preference for different cellular uptake or endocytic pathways [57]. The differences in cell membrane properties of the different cell lines [58] could also affect cellular uptake. The low transfection levels for HepG2 cells can be expected as these cells have a reputation of being a difficult-to-transfect cell line [59], as they often grow in clumps that hinder transfection. The low level of transfection for the pDNA:MgAl 0.25 complex could result from the large size of the pDNA:MgAl 0.25 complex and the possibility of aggregation caused by the pDNA complexing several LDH nanoparticles. This would have induced poor cellular uptake and internalization and, consequently, lower levels of transfection. The MgAl 0.33 LDH carrier showed the highest level of transfection in all cell lines tested. Li and coworkers have also reported that LDHs in a 2:1 ratio showed better adsorption of nucleic acids than those in a 3:1 ratio [32], as seen in this study. It seems that this increased adsorption of nucleic acid corresponded to increased transfection. The amount of the respective amino acids incorporated into the LDH is in keeping with a previous study [27]. The higher degree of amino acid incorporation in the aa-LDHs:pDNA (2:1) appears to have resulted in higher transfection efficiency. His functionalization of the LDHS resulted in better transfection than Arg functionalization, in keeping with reports that propose that incorporating His into gene delivery vehicles improves cellular uptake and enhances endosomal escape through the proton sponge effect [60-62]. Imidazole-containing biomolecules such as histidine have been favored for this reason [63]. However, arginine may have a similar effect, although it was not as pronounced in this study [64, 65]. It was reported that cell-penetrating Arg-rich peptides can passively enter cells by a passive translocation mechanism [66], warranting their further investigation. The results of this study suggest that although the presence of the amino acids did not significantly improve transfection efficiency compared to non-functionalized LDHs, histidine functionalization of the gene delivery vehicle resulted in better transfection than arginine functionalization. Overall, it has been proposed that the ease of loading, anionic exchangeability, and biocompatibility have opened up the avenue for using LDHs as delivery agents in cancer therapy [67].

5. Conclusions

Various analytical techniques confirmed that the co-precipitation method successfully synthesized LDHs and aa-functionalized LDHs. All the synthesized LDHs bound pDNA, producing stable complexes and concurrently providing adequate protection against nuclease digestion. The negative zeta potentials of most of the nucleic acid: LDH nanocomplexes combined with results of the XRD analysis of the pDNA:MgAl 0.33 complex suggests that the nucleic acids bound to the outer surfaces of the LDHs, and did not fully intercalate within the interlayers. Results of the MTT assays indicate that the pDNA:LDH nanocomplexes were well tolerated by all the cell lines tested. Transfection assessed by the luciferase reporter gene assay was found to be cell-line dependent. The highest levels of transgene expression were obtained with the non-functionalized LDH MgAl 0.33. Overall, functionalization of LDHs with positively charged amino acids did not lead to significantly higher luciferase expression levels, suggesting that further optimizations with regards to the amount of the amino acids incorporated into the LDHs may need to be considered to induce proton-sponge capacity and enhanced gene expression. Nevertheless, these LDH complexes show potential as gene delivery vehicles warranting further investigations.

Acknowledgments

The authors acknowledge the members of the Nano-Gene and Drug delivery group for advice and technical support.

Author Contributions

NN, SS and MS conceptualized and designed the research study. NN performed the research. SS and MS were involved in supervision, project administration, and funding acquisition. NN analyzed the data and wrote the draft manuscript. MS reviewed and edited the manuscript. All authors contributed to editorial changes in the manuscript. All authors read and approved the final manuscript.

Funding

This research was funded by the National Research Foundation, South Africa, Grant number 129263.

Competing Interests

The authors have declared that no competing interests exist.

Additional Materials

The following additional materials are uploaded as supplementary figures.

1. Figure S1: The XRD diffractograms of A: MgAlArg 0.25 (a), MgAlHist 0.25(b), MgAl 0.25 (c); and (B) MgAl 0.33 (a), (MgAlArg 0.33 (b), MgAlHist 0.33 (c).

2. Figure S2: FTIR spectra of (A) MgAl 0.25, MgAlArg 0.25 and MgAlHist 0.25; and (B) MgAl 0.33, MgAlArg 0.33 and MgAlHist 0.33.

References

1. Haddad AF, Young JS, Aghi MK. Using viral vectors to deliver local immunotherapy to glioblastoma. Neurosurg Focus. 2021; 50: E4.
2. Dymek M, Sikora E. Liposomes as biocompatible and smart delivery systems-The current state. Adv Colloid Interface Sci. 2022; 309: 102757.
3. Balgobind A, Daniels A, Ariatti M, Singh M. HER2/neu oncogene silencing in a breast cancer cell model using cationic lipid-based delivery systems. Pharmaceutics. 2023; 15: 1190.
4. Habib S, Singh M. Recent advances in lipid-based nanosystems for gemcitabine and gemcitabine-combination therapy. Nanomaterials. 2021; 11: 597.
5. Naicker K, Ariatti M, Singh M. Active targeting of asiaglycoprotein receptor using sterically stabilized lipoplexes. Eur J Lipid Sci Technol. 2016; 118: 1730-1742.
6. Lee DJ, Kessel E, Lehto T, Liu X, Yoshinaga N, Padari K, et al. Systemic delivery of folate-PEG siRNA lipopolyplexes with enhanced intracellular stability for in vivo gene silencing in leukemia. Bioconjug Chem. 2017; 28: 2393-2409.
7. Riley MK, Vermerris W. Recent advances in nanomaterials for gene delivery-a review. Nanomaterials. 2017; 7: 94.
8. Graczyk A, Pawlowska R, Jedrzejczyk D, Chworos A. Gold nanoparticles in conjunction with nucleic acids as a modern molecular system for cellular delivery. Molecules. 2020; 25: 204.
9. Laurini E, Aulic S, Marson D, Fermeglia M, Pricl S. Cationic Dendrimers for siRNA Delivery: An Overview of Methods for In Vitro/In Vivo Characterization | SpringerLink. Des Delivery SiRNA Ther. 2021; 2282: 209-244.
10. Zenze M, Daniels A, Singh M. Dendrimers as modifiers of inorganic nanoparticles for therapeutic delivery in cancer. Pharmaceutics. 2023; 15: 398.
11. Zhao C, Song X, Liu Y, Fu Y, Ye L, Wang N, et al. Synthesis of graphene quantum dots and their applications in drug delivery. J Nanobiotechnol. 2020; 18: 142.
12. Panigrahi BK, Nayak AK. Carbon nanotubes: An emerging drug delivery carrier in cancer therapeutics. Curr Drug Deliv. 2020; 17: 558-576.
13. Rode A, Sharma S, Mishra DK. Carbon nanotubes: Classification, method of preparation and pharmaceutical application. Curr Drug Deliv. 2018; 15: 620-629.
14. Ahmed M, Jiang X, Deng Z, Narain R. Cationic glyco-functionalized single-walled carbon nanotubes as efficient gene delivery vehicles. Bioconjug Chem. 2009; 20: 2017-2022.
15. Mokhosi SR, Mdlalose W, Nhlapo A, Singh M. Advances in the synthesis and application of magnetic ferrite nanoparticles for cancer therapy. Pharmaceutics. 2022; 14: 937.
16. Arif U, Haider S, Haider A, Khan N, Alghyamah AA, Jamila N, et al. Biocompatible polymers and their potential biomedical applications: A review. Curr Pharm Des. 2019; 25: 3608-3619.
17. Jagaran K, Singh M. Copolymer-green-synthesized copper oxide nanoparticles enhance folate-targeting in cervical cancer cells in vitro. Polymers. 2023; 15: 2393.
18. Mijanović O, Branković A, Borovjagin AV, Butnaru DV, Bezrukov EA, Sukhanov RB, et al. Battling neurodegenerative diseases with adeno-associated virus-based approaches. Viruses. 2020; 12: 460.
19. Imani R, Emami SH, Faghihi S. Synthesis and characterization of an octaarginine functionalized graphene oxide nano-carrier for gene delivery applications. Phys. Chem. Chem. 2015; 17: 6328-6339.

20. Jing G, Yang L, Wang H, Niu J, Li Y, Wang S. Interference of layered double hydroxide nanoparticles with pathways for biomedicine applications. Adv Drug Deliv Rev. 2022; 188: 114451.
21. Balcomb B, Singh M, Singh S. Synthesis and characterization of layered double hydroxides and their potential as nonviral gene delivery vehicles. ChemistryOpen. 2015; 4: 137-145.
22. Rojas R, Bedoya DA, Vasti C, Giacomelli CE. LDH nanoparticles: synthesis, size control and applications in nanomedicine. In: Layered Double Hydroxides (LDHs): Synthesis, characterization and applications. Ciudad Universitaria, 5000 Córdoba, Argentina: Departamento de Fisicoquímica, Facultad de Ciencias Químicas, Universidad Nacional de Córdoba. New York, USA: Nova Science Publishers; 2015.
23. Choy JH, Kwak SY, Jeong YJ, Park JS. Inorganic layered double hydroxides as nonviral vectors. Angew Chem Int Ed. 2000; 39: 4041-4045.
24. Xu ZP, Lu GQ. Layered double hydroxide nanomaterials as potential cellular drug delivery agents. Pure Appl Chem. 2006; 78: 1771-1779.
25. Herce HD, Garcia AE, Cardoso MC. Fundamental molecular mechanism for the cellular uptake of guanidinium-rich molecules. J Am Chem Soc. 2014; 136: 17459-17467.
26. Holeček M. Histidine in health and disease: Metabolism, physiological importance, and use as a supplement. Nutrients. 2020; 12: 848.
27. Nundkumar N, Singh S, Singh M. Amino acid functionalized hydrotalcites for gene silencing. J Nanosci Nanotechnol. 2020; 20: 3387-3397.
28. Wang H, Liang XH, Zhao RX, Feng LD, Li H. Spectrophotometric determination of arginine in grape juice using 8-hydroquinoline. Agric Sci China. 2008; 7: 1210-1215.
29. Patel VB, Patel KN, Shah MM, Mayank B. Spectrophotometric determination of histidine hydrochloride monohydrate in pharmaceutical formulations. Int J Pharmtech Res. 2009; 1: 852-856.
30. Singh M. Assessing nucleic acid: Cationic nanoparticle interaction for gene delivery. In: Bio-Carrier Vectors. New York, NY: Humana; 2021. pp. 43-55.
31. Mora M, Jiménez Sanchidrián C, Ruiz JR. Raman spectroscopy study of layered-double hydroxides containing magnesium and trivalent metals. Mater Lett. 2014; 120: 193-195.
32. Li L, Gu W, Chen J, Chen W, Xu ZP. Co-delivery of siRNAs and anti-cancer drugs using layered double hydroxide nanoparticles. Biomaterials. 2014; 35: 3331-3339.
33. Kagunya W, Baddour-Hadjean R, Kooli F, Jones W. Vibrational modes in layered double hydroxides and their calcined derivatives. Chem Phys. 1998; 236: 225-234.
34. Medina-Juárez O, García-Sánchez MÁ, Arellano-Sánchez U, Kornhauser-Straus I, Rojas-González F. Optimal surface amino-functionalization following thermo-alkaline treatment of nanostructured silica adsorbents for enhanced CO2 adsorption. Materials. 2016; 9: 898.
35. Palmer SJ, Frost RL, Spratt HJ. Synthesis and Raman spectroscopic study of Mg/Al, Fe hydrotalcites with variable cationic ratios. J Raman Spectrosc. 2009; 40: 1138-1143.
36. Kloprogge JT, Hickey L, Frost RL. Heating stage Raman and infrared emission spectroscopic study of the dehydroxylation of synthetic Mg-hydrotalcite. Appl Clay Sci. 2001; 18: 37-49.
37. Choi G, Yang JH, Park GY, Vinu A, Elzatahry A, Yo CH, et al. Intercalative ion‐exchange route to amino acid layered double hydroxide nanohybrids and their sorption properties. Eur J Inorg Chem. 2015; 2015: 925-930.

38. Li B, Wu P, Ruan B, Liu P, Zhu N. Study on the adsorption of DNA on the layered double hydroxides (LDHs). Spectrochim Acta A Mol Biomol Spectrosc. 2014; 121: 387-393.
39. Kumar S, Rai SB. Spectroscopic studies of L-arginine molecule. Indian J Pure Appl Phys. 2010; 48: 251-255.
40. Kriven WM, Kwak SY, Wallig MA, Choy JH. Bio-resorbable nanoceramics for gene and drug delivery. MRS Bull. 2004; 29: 33-37.
41. Barth A. The infrared absorption of amino acid side chains. Prog Biophys Mol Biol. 2000; 74: 141-173.
42. Akinyelu J, Oladimeji O, Daniels A, Singh M. Folate-targeted doxorubicin delivery to breast and cervical cancer cells using a chitosan-gold nano-delivery system. J Drug Deliv Sci Technol. 2022; 67: 102978.
43. Lu M, Shan Z, Andrea K, Macdonald B, Beale S, Curry DE, et al. Chemisorption mechanism of DNA on Mg/Fe layered double hydroxides nanoparticles: Insights into engineering effective siRNA delivery systems. Langmuir. 2016; 32: 2659-2667.
44. Nagaraj VJ, Sun X, Mehta J, Martin M, Ngo T, Dey SK. Synthesis, characterization and in vitro drug delivery capabilities of (Zn, Al)-based layered double hydroxide nanoparticle. J Nanotechnol. 2015; 2015: 350370.
45. Jin W, Lee D, Jeon Y, Park DH. Biocompatible hydrotalcite nanohybrids for medical functions. Minerals. 2020; 10: 172.
46. Honary S, Zahir F. Effect of zeta potential on the properties of nano-drug delivery systems-A review (Part 2). Trop J Pharm Res. 2013; 12: 265-273.
47. Desigaux L, Belkacem MB, Richard P, Cellier J, Léone P, Cario L, et al. Self-assembly and characterization of layered double hydroxide/DNA hybrids. Nano Lett. 2006; 6: 199-204.
48. Barichello JM, Kizuki S, Tagami T, Soares LA, Ishida T, Kikuchi H, et al. Agitation during lipoplex formation harmonizes the interaction of siRNA to cationic liposomes. Int J Pharm. 2012; 430: 359-365.
49. Zhang Y, Garzon-Rodriguez W, Manning MC, Anchordoquy TJ. The use of fluorescence resonance energy transfer to monitor dynamic changes of lipid-DNA interactions during lipoplex formation. Biochim Biophys Acta. 2003; 1614: 182-192.
50. Dong H, Parekh HS, Xu ZP. Particle size-and number-dependent delivery to cells by layered double hydroxide nanoparticles. J. Colloid Interface Sci. 2015; 437: 10-16.
51. Matulis D, Rouzina I, Bloomfield VA. Thermodynamics of DNA binding and condensation: Isothermal titration calorimetry and electrostatic mechanism. J Mol Biol. 2000; 296: 1053-1063.
52. Xu ZP. Strategy for cytoplasmic delivery using inorganic particles. Pharm Res. 2022; 39: 1035-1045.
53. Wong Y, Markham K, Xu ZP, Chen M, Lu GQ, Bartlett PF, et al. Efficient delivery of siRNA to cortical neurons using layered double hydroxide nanoparticles. Biomaterials. 2010; 31: 8770-8779.
54. Cunha VR, Ferreira AM, Constantino VR, Tronto J, Valim JB. Layered double hydroxides: Inorganic nanoparticles for storage and release of species of biological and therapeutic interest. Quim Nova. 2010; 33: 159-171.
55. Bejoy N. Hydrotalcite: The clay that cures. Resonance. 2001; 6: 57-61.

56. Mao BH, Luo YK, Wang Jr B, Chen CW, Cheng FY, Lee YH, et al. Use of an in silico knowledge discovery approach to determine mechanistic studies of silver nanoparticles-induced toxicity from in vitro to in vivo. Part Fibre Toxicol. 2022; 19: 6.
57. Vtyurina N, Åberg C, Salvati A. Imaging of nanoparticle uptake and kinetics of intracellular trafficking in individual cells. Nanoscale. 2021; 13: 10436-10446.
58. Spector AA, Yorek MA. Membrane lipid composition and cellular function. J Lipid Res. 1985; 26: 1015-1035.
59. Kim K, Ryu K, Cho H, Shim MS, Cho YY, Lee JY, et al. Effects of decomplexation rates on ternary gene complex transfection with α-Poly (L-lysine) or ε-Poly (L-lysine) as a decomplexation controller in an easy-to-transfect cell or a hard-to-transfect cell. Pharmaceutics. 2020; 12: 490.
60. Joseph C, Daniels A, Singh S, Singh M. Histidine-tagged folate-targeted gold nanoparticles for enhanced transgene expression in breast cancer cells in vitro. Pharmaceutics. 2022; 14: 53.
61. Shi J, Schellinger JG, Johnson RN, Choi JL, Chou B, Anghel EL, et al. Influence of histidine incorporation on buffer capacity and gene transfection efficiency of HPMA-co-oligolysine brush polymers. Biomacromolecules. 2013; 14: 1961-1970.
62. Meng Z, Luan L, Kang Z, Feng S, Meng Q, Liu K. Histidine-enriched multifunctional peptide vectors with enhanced cellular uptake and endosomal escape for gene delivery. J Mater Chem B. 2017; 5: 74-84.
63. Habib S, Singh M, Ariatti M. Glycosylated liposomes with proton sponge capacity: Novel hepatocyte-specific gene carriers. Curr Drug Deliv. 2013; 10: 685-695.
64. Gao Y, Xu Z, Chen S, Gu W, Chen L, Li Y. Arginine-chitosan/DNA self-assemble nanoparticles for gene delivery: In vitro characteristics and transfection efficiency. Int J Pharm. 2008; 359: 241-246.
65. Wang GH, Zhao YZ, Juan TA, Zhu SH, Zhou KC. Arginine functionalized hydroxyapatite nanoparticles and its bioactivity for gene delivery. Trans Nonferrous Met Soc China. 2015; 25: 490-496.
66. Allolio C, Magarkar A, Jurkiewicz P, Baxová K, Javanainen M, Mason PE, et al. Arginine-rich cell-penetrating peptides induce membrane multilamellarity and subsequently enter via formation of a fusion pore. Proc Natl Acad Sci. 2018; 115: 11923-11928.
67. Abdelgalil RM, Khattab SN, Ebrahim S, Elkhodairy KA, Teleb M, Bekhit AA, et al. Engineered sericin-tagged layered double hydroxides for combined delivery of pemetrexed and ZnO quantum dots as biocompatible cancer nanotheranostics. ACS Omega. 2023; 8: 5655-5671.